The Complete Flux Scheme : error analysis and application to plasma simulation

EINDHOVEN UNIVERSITY OF TECHNOLOGY
Department of Mathematics and Computer Science

CASA-Report 12-27
July 2012

The complete flux scheme – error analysis and application to plasma simulation

by

L. Liu, J. van Dijk, J.H.M. ten Thije Boonkkamp,
D.B. Mihailova, J.J.A.M. van der Mullen

Centre for Analysis, Scientific computing and Applications
Department of Mathematics and Computer Science
Eindhoven University of Technology
P.O. Box 513
5600 MB Eindhoven, The Netherlands
ISSN: 0926-4507

The Complete Flux Scheme — Error Analysis and Application to Plasma Simulation

L. Liu[a], J. van Dijk[a], J.H.M. ten Thije Boonkkamp[b], D.B. Mihailova[a], J.J.A.M. van der Mullen[a]

[a] *Department of Applied Physics, Eindhoven University of Technology, P.O. Box 513, 5600 MB Eindhoven, The Netherlands*

[b] *Department of Mathematics and Computer Science, Eindhoven University of Technology, P.O. Box 513, 5600 MB Eindhoven, The Netherlands*

Abstract

The Complete Flux scheme (CFS) (J.H.M. ten Thije Boonkkamp et al., *J. Sci. Comput.* **46** (2011) 47–70) is an extension of the widely used exponential difference scheme for advection-diffusion-reaction equations. In the present paper we provide a rigorous proof that the convergence order of this scheme is 2 for all grid Péclet numbers, whereas that of the exponential scheme reduces to 1 for high grid Péclet numbers in the presence of source terms. The performance of both schemes is compared in two case studies: a model system and a real-world model of a parallel-plate glow discharge. The results indicate that the usage of CFS allows a considerable reduction of the number of grid points that is required to obtain the same accuracy. The MATLAB/Octave source code that has been used in these studies has been made available.

Key words: complete flux scheme, exponential difference scheme, error analysis, plasma model

1. Introduction

Many physical quantities are governed by equations of advection-diffusion-reaction type. Examples are the densities of particles, momentum and energy, which are encountered in chemical and combustion engineering [1], in plasma physics [2, 3] and in semiconductor physics [4]. Such equations can be written as a balance equation for the quantity n of interest, which has the form

$$\frac{\partial n}{\partial t} + \nabla \cdot \mathbf{\Gamma} = s. \tag{1a}$$

Here s is the net volumetric production rate of the quantity, and the flux density vector $\mathbf{\Gamma}$ is given by

$$\mathbf{\Gamma} = \boldsymbol{v} n - D \nabla n, \tag{1b}$$

with $\boldsymbol{v}$ the advection or drift velocity and D the diffusion coefficient.

Analytical solutions of equations (1) exist only for special cases. Therefore one commonly resorts to numerical methods to obtain approximate solutions, typically in the *nodal points* of

a numerical mesh. Such methods require that equation (1a) be discretized in those points. If the finite volume method (FVM) is used, this in turn requires that the longitudinal component of the flux density vector is discretized at an interface point that lies between two adjacent nodal points. Typically, the result of this procedure is an expression for the interface flux density that is linear in the values of n. The key parameter in such expressions is the dimensionless *grid Péclet number* P, which is defined as

$$P = vh/D. \tag{2}$$

Here v is the longitudinal component of $\boldsymbol{v}$ and h is the distance between the nodal points at either side of the interface. The grid Péclet number is a measure for the ratio of the strengths of advection and diffusion: when $|P| \gg 1$ advection is dominant, while for $|P| \ll 1$ diffusion is the dominant transport mechanism.

Many numerical schemes have been developed for the discretization of the flux density. The most popular ones are the central difference, upwind, exponential difference scheme (EDS) [5] and the hybrid scheme [6]. The central difference scheme has the disadvantage that it may produce unphysical oscillating results for $|P| \geq 2$, which poses a restriction on the mesh size h. On the other hand, the upwind scheme does not produce these unphysical oscillations, but the scheme is too diffusive for $|P| \gg 1$, and as a result, the resolution of interior or boundary layers are poor. The hybrid scheme and the more accurate EDS combine the best of both worlds and perform reasonably well for all grid Péclet numbers. Since EDS is more accurate for the intermediate grid Péclet numbers, it is the method of choice in most contemporary simulation studies.

But EDS is not without drawback. One is that its convergence order reduces from 2 to 1 for large $|P|$ in the presence of source terms ($s \neq 0$). This can be attributed to the fact that the derivation of EDS is based on a boundary value problem in which this source term is disregarded.

Recently, Ten Thije Boonkkamp and Anthonissen [7] developed the *complete flux scheme* (CFS), which does take the source term into account. The result is an additional term in the expression for the numerical flux, which manifests itself for large grid Péclet numbers in the presence of source terms. In the absence of source terms, CFS reduces to EDS. The form of CFS, tridiagonal coupling in both n and s, is not rare in literature, especially the schemes for singularly perturbed problems share this property, such as the scheme derived by El-Mistikawy and Werle [8] and the one derived by Stynes and O'Riordan [9]. The latter has very similar expressions and almost the same coefficients (same functions needed in the expressions) as CFS and exhibits second-order accuracy uniformly in grid Péclet number for a singular perturbation problem in conservative form. Nevertheless, they are not identical. Among the differences, e.g., the derivations, the way to calculate the average value of the grid Péclet number on an interval and the right-hand sides of the schemes, etc, the major one is the scope of the application. In Stynes and O'Riordan's scheme the coefficient of the first order derivative term of the problem equation should be positive. This is a considerable limitation for practical applications. For example, for solving the drift-diffusion equations in a model of semiconductors or plasmas, the drift velocity for a species can be positive or negative. CFS does not have this limitation, and we will see it behaves second-order accurate

for the equations, both of electrons and ions in our plasma model. There are some other schemes with this form presented in [10], but from the point of view of plasma simulation, in our opinion CFS is more suitable. For the extension of CFS from stationary problem to time-dependent problem the authors adopted the same approach as in [11] where Hundsdorfer and Verwer extended some well-known schemes, that is, including the time derivative into the source term when discretizing in space. It is proved that in this way the semi-discretization has smaller dissipation and dispersion errors than the one obtained without doing that, see [7].

In [7] the authors found CFS to be second order accurate for all source strengths s and grid Péclet numbers, but failed to prove that this is always the case. In this paper we will establish a rigorous mathematical proof that CFS is second order convergent, uniformly in the grid Péclet number, even in the presence of source terms.

This paper is organized as follows. In Section 2 we will summarize the derivation of CFS. Section 3 provides a detailed error analysis of CFS and proves its second order convergence. In Section 4 the scheme is put to test in two case studies. We first demonstrate its application to a simple boundary value problem with a known analytical solution. Secondly, we apply it to a real-world model of a parallel-plate glow discharge, in which drift-diffusion equations for the ion and electron densities are solved self-consistently with Poisson's equation for the electric field. In both case studies the accuracies of EDS and CFS are compared for various numbers of grid points. The results indicate that the usage of CFS allows a considerable reduction of the number of grid points for a fixed tolerance level. Finally, Section 5 provides conclusions.

2. The complete flux scheme

In this section we outline CFS for a stationary conservation law of advection-diffusion-reaction type in one-dimensional Cartesian coordinate system[1]. In this case equation (1) reduce to

$$\frac{\mathrm{d}}{\mathrm{d}x}\Gamma = s, \tag{3a}$$

$$\Gamma := vn - D\frac{\mathrm{d}n}{\mathrm{d}x}. \tag{3b}$$

Equation (3) is solved on a closed interval $[0, 1]$ covered with a uniform vertex centered grid, depicted in figure 1. The grid size is h and the unknowns are evaluated at the grid points $x_j = jh,\ j = 0, 1, \cdots, N$. In addition, the interfaces of the control volumes lie in the middle between two adjacent grid points.

[1]The scheme has already been extended to two-dimensional, time-dependent problems, and to curvilinear coordinate systems. These extensions are outside the scope of the present paper, we refer to [7, 12] for details.

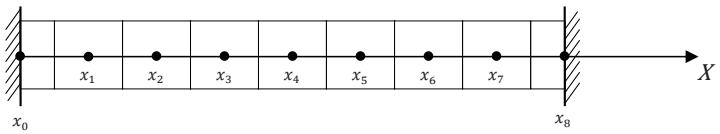

Figure 1: Uniform vertex centered grid. Solid circles denote nodal points and squares denote control volumes.

Integrating over each control volume and adopting the midpoint rule for the integral of s, equation (3) becomes

$$\Gamma_{j+1/2} - \Gamma_{j-1/2} = s_j h, \tag{4}$$

where $\Gamma_{j+1/2}$ is the numerical approximation of the flux at $x = x_{j+1/2}$ and $s_j = s(x_j)$. In CFS, the derivation of $\Gamma_{j+1/2}$ is based on the analytical solution of the following local boundary value problem with appropriate quadrature rules [7]:

$$\frac{\mathrm{d}}{\mathrm{d}x}\left(vn - D\frac{\mathrm{d}n}{\mathrm{d}x}\right) = s, \quad x_j < x < x_{j+1}, \tag{5a}$$

$$n(x_j) = n_j, \quad n(x_{j+1}) = n_{j+1}, \tag{5b}$$

therefore, $\Gamma_{j+1/2}$ not only depends on n but also on s. The numerical flux $\Gamma_{j+1/2}$ can be expressed as

$$\Gamma_{j+1/2} = \Gamma^{\mathrm{h}}_{j+1/2} + \Gamma^{\mathrm{i}}_{j+1/2}, \tag{6a}$$

$$\Gamma^{\mathrm{h}}_{j+1/2} = \alpha_{j+1/2} n_j - \beta_{j+1/2} n_{j+1}, \tag{6b}$$

$$\Gamma^{\mathrm{i}}_{j+1/2} = h(\gamma_{j+1/2} s_j + \delta_{j+1/2} s_{j+1}), \tag{6c}$$

where $\Gamma^{\mathrm{h}}_{j+1/2}$ and $\Gamma^{\mathrm{i}}_{j+1/2}$ are the homogeneous and inhomogeneous part, which correspond to the homogeneous and the particular solution of (5), respectively. The coefficients $\alpha_{j+1/2}$, $\beta_{j+1/2}$, $\gamma_{j+1/2}$ and $\delta_{j+1/2}$ are defined by

$$\begin{aligned}
\alpha_{j+1/2} &:= \frac{\mathcal{D}_{j+1/2}}{h} B(-\bar{P}_{j+1/2}), \\
\beta_{j+1/2} &:= \frac{\mathcal{D}_{j+1/2}}{h} B(\bar{P}_{j+1/2}), \\
\gamma_{j+1/2} &:= \max\left(\frac{1}{2} - W(\bar{P}_{j+1/2}), 0\right), \\
\delta_{j+1/2} &:= \min\left(\frac{1}{2} - W(\bar{P}_{j+1/2}), 0\right), \\
\mathcal{D}_{j+1/2} &:= \frac{\tilde{P}_{j+1/2}}{\bar{P}_{j+1/2}} \tilde{D}_{j+1/2},
\end{aligned} \tag{7}$$

where $\bar{P}_{j+1/2}$ and $\tilde{P}_{j+1/2}$ are the arithmetic average and weighted average of the grid Péclet number, respectively defined as

$$\begin{aligned}
\bar{P}_{j+1/2} &:= \frac{1}{2}(P_j + P_{j+1}), \\
\tilde{P}_{j+1/2} &:= W(-\bar{P}_{j+1/2}) P_j + W(\bar{P}_{j+1/2}) P_{j+1},
\end{aligned}$$

and $\tilde{D}_{j+1/2}$ is the weighted average for D. In addition, the Bernoulli function $B(z)$ and function $W(z)$ are defined by

$$B(z) := \frac{z}{\exp(z)-1}, \quad W(z) := \frac{\exp(z)-1-z}{z(\exp(z)-1)} = \frac{1}{z}\Big(1 - B(z)\Big), \tag{8}$$

and shown in figure 2.

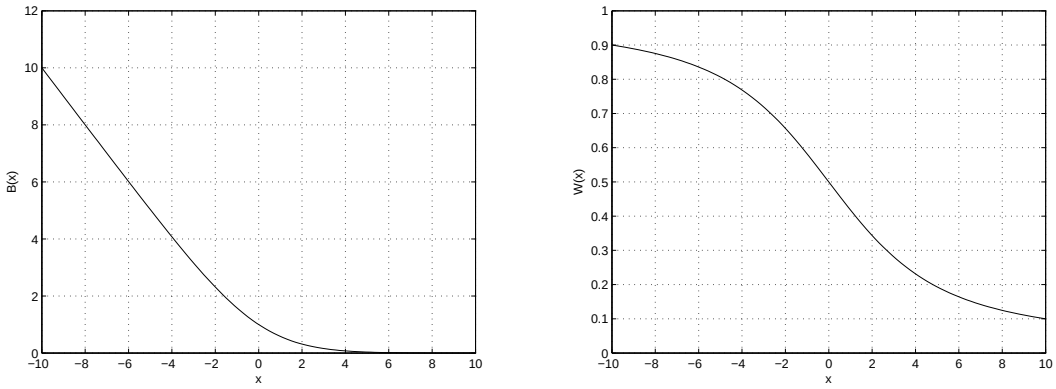

(a) (b)

Figure 2: Bernoulli function $B(z)$ (a) and function $W(z)$ (b).

Substituting (6) into equation (4) we obtain the expression of CFS

$$\mathcal{L}^h n_j = \mathcal{W}^h s_j, \quad j = 1, \cdots, N-1, \tag{9}$$

where the difference operator $\mathcal{L}^h$ and the weighting operator $\mathcal{W}^h$ are defined by

$$\mathcal{L}^h n_j := -a_{W,j} n_{j-1} + a_{C,j} n_j - a_{E,j} n_{j+1}, \tag{10}$$

$$\mathcal{W}^h s_j := b_{W,j} s_{j-1} + b_{C,j} s_j + b_{E,j} s_{j+1}, \tag{11}$$

with coefficients $a_{W,j}, b_{W,j}$ etc. defined by

$$\begin{aligned} a_{W,j} := \frac{1}{h}\alpha_{j-1/2}, \quad a_{E,j} := \frac{1}{h}\beta_{j+1/2}, \quad a_{C,j} := \frac{1}{h}(\alpha_{j+1/2} + \beta_{j-1/2}), \\ b_{W,j} := \gamma_{j-1/2}, \quad b_{E,j} := -\delta_{j+1/2}, \quad b_{C,j} := 1 - \gamma_{j+1/2} + \delta_{j-1/2}. \end{aligned} \tag{12}$$

It is worth mentioning that EDS is a special case of CFS, and it is derived from a homogeneous boundary-value problem with constant coefficients. In the next section we will analyze the accuracy of CFS.

3. Error analysis

In this section we analyze the accuracy of CFS and prove that it is uniformly second-order accurate for the following two-point boundary value problem

$$\mathcal{L}n := vn' - Dn'' = s(x), \quad 0 < x < 1, \tag{13a}$$

$$n(0) = n_{\mathrm{L}}, \quad n(1) = n_{\mathrm{R}}, \tag{13b}$$

where $v > 0$ and $D \in (0, 1]$ are constants and $s \in C^m[0, 1]$. Although we assume $v > 0$, it is not a real restriction, because for the case of $v < 0$ one can transform the problem to $v > 0$ with the change of variable $\bar{x} = 1 - x$.

The coefficients of (13) are constants, so the coefficients in (10) and (11) can be written as, see (7),

$$\begin{aligned} a_W := Dh^{-2}B(-P), \quad a_E := Dh^{-2}B(P), \quad a_C := a_W + a_E, \\ b_W := \frac{1}{2} - W(P), \quad b_E := 0, \quad b_C := \frac{1}{2} + W(P), \end{aligned} \tag{14}$$

where P is the grid Péclet number. In the remainder of this paper, C, c, c_1 and c_2 will be positive constants, independent of h and D, whose values may change from line to line. As usual we investigate stability first and then consistency and convergence.

3.1. Stability

Applying CFS to (13) we obtain the linear system of equations

$$\boldsymbol{An} = \boldsymbol{Bs} + \boldsymbol{b}, \tag{15}$$

where $\boldsymbol{A}$, $\boldsymbol{B} \in \mathbb{R}^{(N-1)\times(N-1)}$ are a tri-diagonal matrix and a lower bi-diagnonal matrix. The terms involving boundary values are included in the vector $\boldsymbol{b}$. Note that matrix $\boldsymbol{A}$ is the same as the one drived from the discretization of (13) by EDS. We have the following lemma about the existence and uniqueness of the solution of system (15) and the monotonicity of $\mathcal{L}^h$.

Lemma 3.1. *System (15) has a unique solution. If $\mathcal{L}^h u_j \le \mathcal{L}^h v_j$, $j = 1, 2, \cdots N-1$, and if $u_0 \le v_0$, $u_N \le v_N$, then $u_j \le v_j$, $j = 1, 2, \cdots, N-1$.*

Proof. The results can be obtained directly from the fact that $\boldsymbol{A} = (a_{ij})$ is an M-matrix. In fact, $\boldsymbol{A}$ is irreducibly diagonally dominant, i.e., $\boldsymbol{A}$ is irreducibe, $|a_{ii}| \ge \sum_{j\neq i} |a_{ij}|$ with strict inequality for at least one row. Hence, $\boldsymbol{A}$ has a positive inverse and of monotone type. This demonstrates that system (15) has a unique solution.

Moreover, for $j = 2, 3, \cdots, N-2$, $(\boldsymbol{Av})_j = \mathcal{L}^h v_j$, then the monotonicity of $\boldsymbol{A}$ implies that of $\mathcal{L}^h$. For the points next to the boundaries, e.g., x_1, $\mathcal{L}^h u_1 \le \mathcal{L}^h v_1$ implies

$$a_C(u_1 - v_1) - a_E(u_2 - v_2) \le a_W(u_0 - v_0) \le 0,$$

i.e.,

$$(\boldsymbol{A}\boldsymbol{u})_1 \leq (\boldsymbol{A}\boldsymbol{v})_1.$$

Likewise,

$$(\boldsymbol{A}\boldsymbol{u})_{N-1} \leq (\boldsymbol{A}\boldsymbol{v})_{N-1}.$$

In conclusion, $\mathcal{L}^h u_j \leq \mathcal{L}^h v_j$ implies $u_j \leq v_j$, $j = 1, 2, \cdots, N-1$ under the condition of the lemma. This completes the proof. □

We denote the truncation error and the discretization error of CFS by $\boldsymbol{\tau}$ and $\boldsymbol{e}$, respectively. Then from (15) we have

$$\boldsymbol{e} = \boldsymbol{A}^{-1}\boldsymbol{\tau}. \tag{16}$$

If $\|\boldsymbol{A}^{-1}\|_\infty$ is bounded, then CFS is stable.

Lemma 3.2. *There exists a constant $C > 0$, such that*

$$\|\boldsymbol{A}^{-1}\|_\infty \leq -\frac{1}{v}\left(\frac{1}{R}\ln B(R) + W(R)\right) \leq C, \tag{17}$$

where $R = v/D$.

Proof. From theorem 1.14 in [13] we know that if there is a vector $\boldsymbol{\omega}$ such that

$$\boldsymbol{A}\boldsymbol{\omega} \geq \mathbf{1},$$

where the inequality $\boldsymbol{a} \geq \boldsymbol{b}$ means $a_j \geq b_j$, for all j and $\mathbf{1}$ denotes a column vector whose components are all equal to 1, then

$$\|\boldsymbol{A}^{-1}\|_\infty \leq \|\boldsymbol{\omega}\|_\infty.$$

Actually, as a result of that $\boldsymbol{A}$ is a M-matrix we have

$$\begin{aligned}\|\boldsymbol{A}^{-1}\|_\infty &= \max_i \sum_j \left|(A^{-1})_{ij}\right| = \max_i \left|\sum_j (A^{-1})_{ij}\right| \\ &= \max_i \left|(\boldsymbol{A}^{-1}\mathbf{1})_i\right| \leq \max_i |\omega_i| = \|\boldsymbol{\omega}\|_\infty.\end{aligned}$$

Now we construct a vector $\boldsymbol{\omega}$ that satisfies this criterium. To that end we define the function

$$\omega(x) = \frac{x}{v} - \frac{\exp(Rx) - 1}{v(\exp(R) - 1)}.$$

This is the exact solution of the boundary value problem

$$\begin{aligned} v\omega' - D\omega'' = 1, \quad 0 < x < 1, \\ \omega(0) = 0, \quad \omega(1) = 0. \end{aligned}$$

The first term of $\omega(x)$ is the particular solution of the above problem and the second term is constructed by the general solution of the homogeneous equation. It can easily be shown that $\omega(x) \geq 0$ on $[0,1]$ and it obtains the maximal value in the unique stationary point $x^* = -\ln B(R)/R \in (0,1)$, where function B is defined in (8).

Let $\boldsymbol{\omega}$ be the restriction of ω to the grid. One can verify that

$$\mathcal{L}^h\left(\frac{x_j}{v}\right) = 1,\ \mathcal{L}^h \exp(Rx_j) = 0 \text{ and } \mathcal{L}^h 1 = 0.$$

Therefore,

$$\boldsymbol{A}\boldsymbol{\omega} = \mathbf{1}.$$

As a result we have

$$\begin{aligned}\|\boldsymbol{A}^{-1}\|_\infty \leq \|\boldsymbol{\omega}\|_\infty \leq \|\omega\|_\infty &= \omega(x^*) \\ &= -\frac{1}{v}\left(\frac{1}{R}\ln B(R) + W(R)\right),\end{aligned}$$

where function W is defined in (8). In addition, if $v = 1$, then $\omega(x^*) \to 1$ as $D \to 0$. Therefore, $\|\boldsymbol{A}^{-1}\|_\infty$ is bounded. □

Remark 3.3. *In (17), if $D = 1$, then $\|\boldsymbol{A}^{-1}\|_\infty \leq 1/8$ as $v \to 0$ as expected, because when $D = 1$ CFS reduces to the central difference scheme as $v \to 0$. Additionally, $\|\boldsymbol{A}^{-1}\|_\infty \leq 1/8$ for the central difference scheme [13].*

3.2. Consistency

To investigate the convergence of CFS we need to estimate the truncation error first. The truncation error is defined to be

$$\tau_j := \mathcal{L}^h n(x_j) - \mathcal{W}^h(\mathcal{L}n)(x_j) \ \text{ for } j = 1, 2\cdots, N-1. \tag{18}$$

We derive its expression in two cases, viz, for $h \leq D$ and $D \leq h$, by using the Taylor expansion

$$f(x_2) = \sum_{k=0}^{q} \frac{f^{(k)}(x_1)}{k!}(x_2 - x_1)^k + R_q(x_1, x_2; f), \tag{19}$$

where the remainder $R_q(x_1, x_2; f)$ is given by

$$R_q(x_1, x_2; f) = \frac{1}{q!}\int_{x_1}^{x_2} (x_2 - x)^q f^{(q+1)}(x)\mathrm{d}x, \tag{20}$$

for a sufficiently smooth function $f(x)$.

First, for the case $h \leq D$ using the Taylor expansion (19) up to the fourth derivative of n we obtain the following expression for the truncation error

$$\tau_j = T_3 n^{(3)}(x_j) + I_1 + I_2 + I_3 + I_4. \tag{21}$$

One can easily check that the leading term

$$T_3 = \frac{vh^2}{6} - \Big(\frac{1}{2} - W(P)\Big)(Dh + \frac{1}{2}vh^2),$$

and the remainder terms

$$\begin{aligned}
I_1 &= -Dh^{-2}B(-P)R_3(x_j, x_j - h; n),\\
I_2 &= -Dh^{-2}B(P)R_3(x_j, x_j + h; n),\\
I_3 &= -v\left(\frac{1}{2} - W(P)\right)R_2(x_j, x_j - h; n'),\\
I_4 &= D\left(\frac{1}{2} - W(P)\right)R_1(x_j, x_j - h; n'').
\end{aligned}$$

Second, for the case $h \geq D$ it suffices to expand up to the third derivative of n, because D contributes one order in the estimation. Then the truncation error can be written as

$$\tau_j = I_1 + I_2 + I_3 + I_4, \tag{22}$$

where

$$\begin{aligned}
I_1 &= -Dh^{-2}B(-P)R_2(x_j, x_j - h; n),\\
I_2 &= -Dh^{-2}B(P)R_2(x_j, x_j + h; n),\\
I_3 &= -v\Big(\frac{1}{2} - W(P)\Big)R_1(x_j, x_j - h; n'),\\
I_4 &= D\Big(\frac{1}{2} - W(P)\Big)R_0(x_j, x_j - h; n'').
\end{aligned}$$

We consider a special case first. If the derivatives of the solution $n(x)$ are uniformly bounded, then from the expression of the truncation error (21) and (22) we can derive the following lemma directly.

Lemma 3.4. *Let $n(x)$ be the solution of (13). If the first four derivatives of $n(x)$ are uniformly bounded, then*

$$|\tau_j| \leq Ch^2. \tag{23}$$

This lemma, along with lemma 3.2, demonstrates the second order convergence of CFS. But the derivatives of the solution are not always bounded, e.g., when a inner or boundary layer exists. Then for the estimation of the truncation error we need the following lemma, given in [14], to bound the dirivatives.

Lemma 3.5. *Let n be the solution of (13). Then it can be decomposed as*

$$n(x) = \gamma y(x) + z(x), \tag{24}$$

where $|\gamma| \leq c_1$ and $y(x) = \exp(-vD^{-1}(1-x))$, and

$$|z^{(i)}(x)| \leq c_2\Big(1 + D^{-i+1}\exp(-vD^{-1}(1-x))\Big), \tag{25}$$

with $c_1 > 0$ and $c_2 > 0$, independent of D.

From (24) we know that the solution $n(x)$ of (13) can be decomposed into two terms. For the first term, one can easily verify that $y(x)$ is a solution of the homogeneous equation of (13). In addition, CFS is exact for the constant coefficient homogeneous problem. As a result, the truncation error from this term is zero. Therefore, the truncation error can be written as

$$\tau_j = \mathcal{L}^h z(x_j) - \mathcal{W}^h(\mathcal{L}z)(x_j) \quad \text{for } j = 1, 2 \cdots, N-1. \tag{26}$$

Now we start estimating the terms of (21) for the case $h \leq D$. For the first term we have

$$\begin{aligned}
|T_3 z^{(3)}(x_j)| &= \left| \left[\frac{vh^2}{6} - \left(\frac{1}{2} - W(P) \right) \frac{1}{2} vh^2 - \left(\frac{1}{2} - W(P) \right) Dh \right] z^{(3)}(x_j) \right| \\
&\leq \left[\frac{vh^2}{6} + \frac{1}{4} vh^2 + \left(\frac{1}{2} - W(P) \right) \frac{vh^2}{P} \right] |z^{(3)}(x_j)| \\
&\leq \left[\frac{vh^2}{6} + \frac{1}{4} vh^2 + \frac{1}{12} vh^2 + \mathcal{O}(h^4) \right] |z^{(3)}(x_j)| \\
&\leq Ch^2 \big(1 + D^{-2} y(x_j) \big).
\end{aligned}$$

Here we used the Taylor expansion for $1/2 - W(P)$ and the upper bound for $z^{(3)}(x_j)$ given by (25).

For the remainder terms because of the similarity we only present the estimation of $I_1 + I_2$, which is given by

$$\begin{aligned}
|I_1 + I_2| &\leq Dh^{-2} B(-P) \frac{1}{6} \left| \int_{x_j}^{x_j - h} (x_j - h - t)^3 z^{(4)}(t) \mathrm{d}t \right| \\
&\quad + Dh^{-2} B(P) \frac{1}{6} \left| \int_{x_j}^{x_j + h} (x_j + h - t)^3 z^{(4)}(t) \mathrm{d}t \right| \\
&\leq \left(\frac{Dh}{6} [B(-P) + B(P)] \right) \int_{x_j - h}^{x_j + h} |z^{(4)}(t)| \mathrm{d}t \\
&\leq \frac{h}{3} \big(vh \left(\frac{1}{2} - W(P) \right) + D \big) \int_{x_j - h}^{x_j + h} |z^{(4)}(t)| \mathrm{d}t \\
&\leq C(Dh + h^2) \int_{x_j - h}^{x_j + h} |z^{(4)}(t)| \mathrm{d}t \\
&\leq C(Dh + h^2) \int_{x_j - h}^{x_j + h} 1 + D^{-3} \exp(-vD^{-1}(1 - t)) \mathrm{d}t \\
&\leq C(Dh + h^2) \big(h + D^{-2} v^{-1} \sinh(vhD^{-1}) \exp(-vD^{-1}(1 - x_j)) \big).
\end{aligned}$$

Since $\sinh(t) \leq Ct$ for t bounded, we can obtain

$$\begin{aligned}
|I_1 + I_2| &\leq C(Dh + h^2)(h + D^{-3} h) \exp(-vD^{-1}(1 - x_j)) \\
&\leq Ch^2 (1 + D^{-2} y(x_j)).
\end{aligned}$$

Here we used the relation

$$\frac{D}{2}\big(B(P)+B(-P)\big)=vh\big(\frac{1}{2}-W(P)\big)+D.$$

Similarly we can estimate I_3 and I_4 and the upper bounds have the same forms.

Then for $h \geq D$, we estimate the terms of (22). As an example, the estimation process of I_1 is presented.

$$\begin{aligned}
|I_1| &\leq \left| Dh^{-2}B(-P)\frac{1}{2}\int_{x_j}^{x_j-h} h^2 z^{(3)}(t)\mathrm{d}t \right| \\
&\leq D\big(B(P)+P\big)\frac{1}{2}\int_{x_j-h}^{x_j} |z^{(3)}(t)|\mathrm{d}t \\
&\leq CD\int_{x_j-h}^{x_j} 1+D^{-2}y(t)\mathrm{d}t + Ch\int_{x_j-h}^{x_j} 1+D^{-2}y(t)\mathrm{d}t \\
&\leq C\big(h^2+hD^{-1}v^{-1}y(x_j)\big)\big(1-\exp(-vD^{-1}h)\big) \\
&+ C\big(hD+v^{-1}y(x_j)\big)\big(1-\exp(-vD^{-1}h)\big) \\
&\leq C\big(h^2+hD^{-1}y(x_j)\big) \\
&\leq C\big(h^2+\left(\frac{D}{h}\right)\left(\frac{h}{D}\right)^2 y(x_j)\big) \\
&\leq C\big(h^2+Dh^{-1}y(x_{j+1})\big).
\end{aligned}$$

Here we used the inequality $t^k \leq C\exp(t)$, for a positive integer k. Similarly, we can estimate the terms I_2, I_3 and I_4 and they have the same forms of the upper bounds as I_1. In summary, we have the following lemma for the truncation error.

Lemma 3.6. *If the derivatives of $n(x)$ up to the fourth order exist, then the truncation error of CFS satisfies*

$$|\tau_j| \leq Ch^2 + Ch^2D^{-2}\exp(-vD^{-1}(1-x_j)), \quad h \leq D, \tag{27}$$

$$|\tau_j| \leq Ch^2 + CDh^{-1}\exp(-vD^{-1}(1-x_{j+1})), \quad h \geq D. \tag{28}$$

3.3. Convergence

Our aim is to prove that CFS is uniformly second-order convergent for problem (13). The principal result can be summarized as

Theorem 3.7. *There is a constant C, independent of D and h, such that*

$$|e_j| \leq Ch^2, \tag{29}$$

for all $D \in (0,1]$ and $v > 0$.

To prove this theorem we adopt the comparison function approach, which was employed in [14, 15, 16] for analysis of some difference methods for singular perturbation problems. An outline is given in [15]. For our problem we choose the comparison functions $\phi(x) = 1+x$ and $\psi(x) = \exp(-\lambda D^{-1}(1-x))$ for some $\lambda > 0$. The function ϕ is used to estimate the error where n is "well behaved", while ψ estimates the error "near" the layer. The error estimate is obtained using ϕ, ψ, and bounds on the truncation error. Lower bounds of $\mathcal{L}^h\phi(x_j)$ and $\mathcal{L}^h\psi(x_j)$ play important roles in this approach and they are given in the following two lemmas.

Lemma 3.8. *There is a constant C, such that $\mathcal{L}^h\phi(x_j) \geq C$ for $D \in (0, 1]$ and $v > 0$.*

The proof of lemma 3.8 is straightforward, so it is omitted.

Lemma 3.9. *There exists constants c_1 and c_2 such that $h \leq c_1$ and $0 < \lambda \leq c_2$, for some constant C, it holds*

$$\mathcal{L}^h\psi(x_j) \geq CD^{-1}\psi(x_j), \text{ for } h \leq D, \tag{30}$$

$$\mathcal{L}^h\psi(x_j) \geq Ch^{-1}\psi(x_j), \text{ for } h \geq D. \tag{31}$$

Proof. The results follow immediately from the proof of lemma 3.6 in [16], once the following expression is observed,

$$\begin{aligned}\mathcal{L}^h\psi(x_j) &= -a_W \exp(-\lambda D^{-1}(1 - x_{j-1})) \\ &\quad + (a_W + a_E)\exp(-\lambda D^{-1}(1 - x_j)) - a_E \exp(-\lambda D^{-1}(1 - x_{j+1}) \\ &= a_W\psi(x_{j+1})\big(\exp(-\lambda h D^{-1}) - a_E/a_W\big)\big(1 - \exp(-\lambda h D^{-1})\big).\end{aligned}$$

The idea is to estimate the individual factors in the above expression for the three cases (1) $h/D \leq c$, (2) $h/D \geq C$ and (3) $c \leq h/D \leq C$ (for appropriately chosen c and C). □

From lemma 3.6 we see that the truncation error in the case $h \leq D$ is second order, but in the case $h \geq D$, the order can not be determined. So we can not determine the convergence order from it. Nevertheless, we can obtain a preliminary result for the discretization error. Along with lemma 3.8, 3.9 and 3.1 we have the following theorem.

Theorem 3.10. *Let $\{n_j\}$ be the approximate solution of (13) using CFS. Then there are a constant λ, which depends only on v, and a constant C, which is independent of D and h, such that*

$$|n(x_j) - n_j| \leq Ch^2 + Ch^2D^{-1}\exp(-\lambda D^{-1}(1 - x_j)), \quad h \leq D, \tag{32}$$

$$|n_j - n(x_j)| \leq Ch^2 + CD\exp(-\lambda D^{-1}(1 - x_{j+1})), \quad D \leq h. \tag{33}$$

Proof. We consider the case $h \leq D$. From (27) by choosing a $\lambda \leq v$ we have

$$\begin{aligned}|\tau_j| &= |\mathcal{L}^h(n(x_j) - n_j)| \\ &\leq Ch^2 + Ch^2D^{-2}\exp(-\lambda D^{-1}(1 - x_j)) \\ &\leq Ch^2\mathcal{L}^h\phi(x_j) + Ch^2D^{-1}\mathcal{L}^h\psi(x_j) \\ &= \mathcal{L}^h[Ch^2\phi(x_j) + Ch^2D^{-1}\psi(x_j)].\end{aligned}$$

Then (32) follows from lemma 3.1. The second estimation can be obtained similarly. □

It is not sufficient to prove theorem 3.7 from theorem 3.10. We still need another lemma which gives a three-term decomposition of the solution $n(x)$ of (13) by using the two-variable expansion method (see [17] and references therein).

Lemma 3.11. *The solution $n(x)$ of (13) can be written in the form*

$$n(x) = A_0(x) + B_0 \exp(-vD^{-1}(1-x)) + DR_0(x;D), \tag{34}$$

where the constant B_0 and the norm of $A_0 \in C^{m+1}[0,1]$ depend on the boundary values of (13) and the integral of $s(x)$. The function $R_0(x)$ satisfies the following problem

$$-DR_0'' + vR_0' = F_0(x), \quad R_0(0;D) = \kappa_0(D), \ R_0(1;D) = 0, \tag{35}$$

where $\kappa_0(D)$ is bounded and $F_0 \in C^{m-1}[0,1]$.

Proof. Omitted here, see [17]. □

After all those preparation we can prove theorem 3.7.

Proof. From lemma 3.11 we know that theorem 3.7 holds if the contribution of the three terms of (34) to the discretization error are uniformly $\mathcal{O}(h^2)$. The contribution of A_0 is bounded by Ch^2. In fact, its derivatives are uniformly bounded, thus the truncation error is uniformly $\mathcal{O}(h^2)$ from lemma 3.4. This, along with lemma 3.2, implies the statement. For the third summand DR_0, from lemma 3.11 we know that the discretization error of R_0 from using CFS has the estimation (32) and (33), thus the contribution of DR_0 is uniformly $\mathcal{O}(h^2)$. The second term of (34) is the analytical solution of the homogeneous equation of (13), so its contribution to the discretization error is zero. This completes the proof. □

4. Case Studies

In this section we apply CFS and EDS to a simple boundary value problem with known analytical solution and to a plasma model to assess and compare the accuracies and efficiencies of the both schemes.

4.1. Advection-diffusion-reaction equation with boundary layer at outflow

In the first case study we solve the following boundary value problem [18]:

$$\begin{aligned} (vn - Dn')' = s, \quad 0 < x < 1, \\ n(0) = 0, \ n(1) = 1, \end{aligned}$$

with a source term s that is chosen such that the exact solution is given by

$$n(x) = a \sin \pi x + \frac{\exp\left(\frac{v}{D}(x-1)\right) - \exp(-\frac{v}{D})}{1 - \exp(-\frac{v}{D})}.$$

Note that for $0 < D \ll 1$ the solution has a thin boundary layer of width D near $x = 1$. We choose the parameter values $v = 1$ and $a = 0.2$. To test whether CFS is second order

uniformly in grid Péclet number, we choose $D = h^p$ for various values of p and compute the maximum of the discretization errors defined by $e_h := \max_j |n(x_j) - n_j|$ and their quotients $e_h/e_{h/2}$ from two consecutive grids.

The results are presented in table 1 and 2 for CFS and EDS, respectively. 1 shows that the CFS is uniformly second order in the grid Péclet number. It agrees with the conclusion of the error analysis. The results in table 2 show that EDS is second order for diffusion-dominated problems but for advection-dominated problems it is only first-order accurate.

Table 1: Maximum discretization errors and quotients $\epsilon_h/\epsilon_{h/2}$ of CFS with various number of grid points and parameter D. Other parameters are: $v = 1$ and $a = 0.2$.

	$D = 1$		$D = h^{0.5}$		$D = h$		$D = h^2$		$D = h^5$	
N	e_h	$e_h/e_{h/2}$	e_h	$e_h/e_{h/2}$	e_h	$e_h/e_{h/2}$	e_h	$e_h/e_{h/2}$	e_h	$e_h/e_{h/2}$
10	1.569e-3	3.91	1.378e-3	3.78	7.968e-4	3.85	1.502e-3	3.73	1.648e-3	4.01
20	4.013e-4	3.95	3.641e-4	3.85	2.069e-4	3.92	4.023e-4	3.93	4.114e-4	4.00
40	1.015e-4	3.98	9.455e-5	3.90	5.280e-5	3.96	1.022e-4	3.98	1.028e-4	4.00
80	2.554e-5	3.99	2.425e-5	3.93	1.334e-5	3.98	2.567e-5	4.00	2.570e-5	4.00
160	6.406e-6	3.99	6.171e-6	3.95	3.352e-6	3.99	6.423e-6	4.00	6.426e-6	4.00
320	1.604e-6		1.561e-6		8.402e-7		1.606e-6		1.606e-6	

Table 2: Maximum discretization errors and quotients $\epsilon_h/\epsilon_{h/2}$ of EDS with various number of grid points and parameter D. Other parameters are: $v = 1$ and $a = 0.2$.

	$D = 1$		$D = h^{0.5}$		$D = h$		$D = h^2$		$D = h^5$	
N	ϵ_h	$\epsilon_h/\epsilon_{h/2}$	ϵ_h	$\epsilon_h/\epsilon_{h/2}$	ϵ_h	$\epsilon_h/\epsilon_{h/2}$	ϵ_h	$\epsilon_h/\epsilon_{h/2}$	ϵ_h	$\epsilon_h/\epsilon_{h/2}$
10	1.522e-3	3.98	8.738e-4	2.51	7.091e-3	1.59	4.934e-2	1.75	6.179e-2	1.98
20	3.827e-4	4.00	3.481e-4	1.75	4.450e-3	1.83	2.815e-2	1.89	3.129e-2	1.99
40	9.561e-5	4.00	1.985e-4	2.41	2.437e-3	1.93	1.491e-2	1.95	1.569e-2	2.00
80	2.391e-5	4.00	9.288e-5	2.38	1.262e-3	1.97	7.656e-3	1.97	7.852e-3	2.00
160	5.976e-6	4.00	3.898e-5	2.54	6.394e-4	1.99	3.878e-3	1.99	3.927e-3	2.00
320	1.494e-6		1.534e-5		3.212e-4		1.951e-3		1.963e-3	

4.2. Plasma model

In the second case study we consider a model for a parallel-plate gas discharge in Helium. It is based on the Local Field Approximation (LFA) model [19], in which the transport coefficients and the ionization rate coefficient depend only on the value of the reduced electric field E/N_g, the magnitude of the electric field divided by the density of the background gas. This type of model is used to simulate a discharge sustained by the secondary emission of

electrons from the cathode. The discharge is formed between two parallel infinitely large planar electrodes, as shown in figure 3.

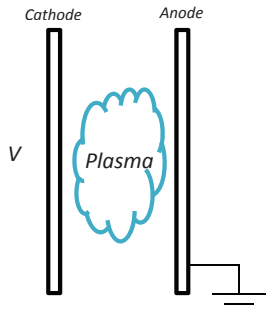

Figure 3: Schematic diagram of DC discharge.

We assume that the background gas Helium is weakly ionized and that its temperature T_g and density N_g are not affected by the formation of a discharge. The time-evolution of the densities n_p of the ions and electrons is described by continuity equations, the flux densities $\mathbf{\Gamma}_p$ are given by the drift-diffusion equation:

$$\frac{\partial n_p}{\partial t} + \nabla \cdot \mathbf{\Gamma}_p = s, \tag{36a}$$

$$\mathbf{\Gamma}_p = \boldsymbol{v}_p n_p - D_p \nabla n_p, \tag{36b}$$

where $p =$ i or e for ions and electrons, respectively. The first term in expression (36b) represents the flux due to the electric field (drift), the second is the flux due to density gradients (diffusion). The drift velocity is given by $\boldsymbol{v}_p = \mu_p \boldsymbol{E}$ where the coefficients μ_p are the species' mobilities and $\boldsymbol{E}$ is the electric field. Only electron impact ionization is considered in our model, so that the source term is given by $s = n_\mathrm{e} N_\mathrm{g} K$, where K is the ionization rate coefficient.

The electric field $\boldsymbol{E}$ depends on the space charge density according to Poisson's equation

$$\nabla \cdot (\varepsilon_0 \boldsymbol{E}) = -\nabla \cdot (\varepsilon_0 \nabla V) = q(n_\mathrm{i} - n_\mathrm{e}), \tag{37}$$

where ε_0 is the dielectric permittivity, V the electrostatic potential and q the elementary charge.

We use the expressions for the particle fluxes at the boundaries as the boundary conditions. The ion flux directed towards the electrode is given by

$$\mathbf{\Gamma}_\mathrm{i} \cdot \hat{\boldsymbol{n}} = a_\mathrm{i} \mu_\mathrm{i} (\boldsymbol{E} \cdot \hat{\boldsymbol{n}}) n_\mathrm{i} + \frac{1}{4} v_{\mathrm{th,i}} n_\mathrm{i}, \tag{38}$$

where $\hat{\boldsymbol{n}}$ is unit outward vector and $v_{\mathrm{th,i}}$ is the thermal velocity of ions, given by

$$v_{\mathrm{th,i}} = \left(\frac{8 K_\mathrm{B} T_\mathrm{i}}{\pi m_\mathrm{i}} \right)^{1/2}, \tag{39}$$

where K_B is the Boltzmann constant, m_i the mass of Helium ions and T_i the temperature of ions. The parameter a_i is set to 1 if the drift velocity $\mu_\mathrm{i}\boldsymbol{E}$ is directed towards the walls and to 0 otherwise, i.e.,

$$a_\mathrm{i} = \begin{cases} 1 & \text{if } \mu_\mathrm{i}\boldsymbol{E}\cdot\hat{\boldsymbol{n}} > 0, \\ \\ 0 & \text{if } \mu_\mathrm{i}\boldsymbol{E}\cdot\hat{\boldsymbol{n}} \leq 0. \end{cases} \tag{40}$$

For electrons, the flux directed towards the electrodes has the same form as (38), but an additional term due to secondary emission is added,

$$\boldsymbol{\Gamma}_\mathrm{e}\cdot\hat{\boldsymbol{n}} = a_\mathrm{e}\mu_\mathrm{e}(\boldsymbol{E}\cdot\hat{\boldsymbol{n}})n_\mathrm{e} + \frac{1}{4}v_{\mathrm{th,e}}n_\mathrm{e} - \gamma_\mathrm{i}\boldsymbol{\Gamma}_\mathrm{i}\cdot\hat{\boldsymbol{n}}, \tag{41}$$

where the secondary emission coefficient γ_i is the average number of electrons emitted per incident ion.

For Poisson's equation (37) the voltages applied to the electrodes provide Dirichlet boundary conditions.

4.2.1. Numerical methods

To show the advantages of CFS we will adopt CFS and EDS for the continuity equation (36) and the central difference scheme for Poission's equation (37). Moreover, for time integration we use the implicit Euler method.

The boundary conditions can be written in a generic expression in one dimension as follows:

$$\Gamma = v_\mathrm{b}n - s_\mathrm{b}, \tag{42}$$

where, for example, for the electron flux (41) on the left boundary

$$v_{\mathrm{b,left}} = a_{\mathrm{e,left}}\mu_{\mathrm{e},0}E_0 + \frac{1}{4}v_{\mathrm{th,e,left}},$$

and

$$s_{\mathrm{b,left}} = \gamma_\mathrm{i}\Gamma_{\mathrm{i},0}.$$

Note that for ions $s_\mathrm{b} = 0$, because there is no secondary emission for ions.

To discretize the transport term in the continuity equation in space, integrating equation (36a) over each control volume and adopting the midpoint rule we obtain the following expression

$$\left(\frac{\partial n}{\partial t}\right)_j h + \Gamma_{j+1/2} - \Gamma_{j-1/2} = s_j h. \tag{43}$$

Substituting the complete flux (6) and applying the implicit Euler method for time integration the following linear system of equations can be obtained

$$(\boldsymbol{J} + \Delta t\boldsymbol{A})\boldsymbol{n}^{k+1} = \boldsymbol{J}\boldsymbol{n}^k + \Delta t\boldsymbol{B}\boldsymbol{s} + \Delta t\boldsymbol{b}, \tag{44}$$

where $\boldsymbol{n}$ is the vector of unknowns, $\boldsymbol{s}$ source term restricted to the grid points, and the vector $\boldsymbol{b}$ contains the boundary data. Both matrices $\boldsymbol{A}$ and $\boldsymbol{B}$ are tridiagonal and given by

$$\boldsymbol{A} = \begin{pmatrix} a_{W,1} - \frac{v_{\mathrm{b,left}}}{h} & -a_{E,0} & & & & \\ -a_{W,1} & a_{C,1} & -a_{E,1} & & & \\ & \ddots & \ddots & \ddots & & \\ & & -a_{W,N-1} & a_{C,N-1} & -a_{E,N-1} & \\ & & & -a_{W,N} & a_{E,N-1} + \frac{v_{\mathrm{b,right}}}{h} \end{pmatrix},$$

$$\boldsymbol{B} = \begin{pmatrix} 1/2 - b_{W,1} & b_{E,0} & & & & \\ b_{W,1} & b_{C,1} & b_{E,1} & & & \\ & \ddots & \ddots & \ddots & & \\ & & b_{W,N-1} & b_{C,N-1} & b_{E,N-1} & \\ & & & b_{W,N} & 1/2 - b_{E,N-1} \end{pmatrix},$$

where the coefficients $a_{W,j}, b_{W,j}$ etc. are defined in (12),

$$\boldsymbol{J} = \mathrm{diag}\,(1/2, 1, \cdots, 1, 1/2)\,,$$

and

$$\boldsymbol{b} = \left(-\frac{s_{\mathrm{b,left}}}{h}, 0, \cdots, 0, \frac{s_{\mathrm{b,right}}}{h}\right)^{\mathrm{T}}.$$

In the expression for the source term s we have used the following expression for n_{e}, which is based on equation (65) and (67) of Ref. [20],

$$n_{\mathrm{e}}^{k+1} = \begin{cases} \frac{|\Gamma_{\mathrm{e}}^k|}{\mu_{\mathrm{e}}^k E^k}, & \text{if } E^k \neq 0, \\ \\ n_{\mathrm{e}}^k, & \text{if } E^k = 0. \end{cases} \tag{45}$$

Note that the coefficient matrix $\boldsymbol{J} + \Delta t \boldsymbol{A}$ of system (44) is tridiagonal and a good choice to solve this system is the tridiagonal matrix algorithm (TDMA), see [21].

Finally, Poisson's equation is discretized by the second order central difference scheme:

$$\varepsilon_0 \left(\frac{\partial^2 V}{\partial x^2}\right)_j \doteq \varepsilon_0 \frac{V_{j+1} - 2V_j + V_{j-1}}{h^2}. \tag{46}$$

The reason that we use the central difference scheme for Poisson's equation is that it only has the second order term, for this kind of equation CFS reduces to the central difference scheme.

For time integration the first-order implicit Euler method does not not affect the accuracy of the solution because our aim is to obtain the steady state. To eliminate other factors affecting the accuracy of the solution we did not apply the so-called semi-implicit treatment [22, 23, 24] for Poisson's equation to circumvent the time step restriction. Instead, a fixed

time step $\Delta t = 10^{-9}$ is imposed. In the time integration Gummel iteration [25] is adopted. The solution procedure is as follows. First, Poisson's equation is solved and then the variables depending on the electric field, e.g., mobility, impact ionization coefficient and electron mean energy are updated from the software named BOLSIG+ [20]. In addition, the diffusion coefficient D is calculated from the mobility by the Einstein relation $D_p = \mu_p K_\mathrm{B} T_p / q$. After that the continuity equations for ions and electrons are solved. At last the flux densities are calculated. Then the calculation proceeds to the next time step. Other parameters used in the model are given in the table 3. Moreover, the density of the background gas N_g is calculated by the ideal gas law $N_\mathrm{g} = p/(K_\mathrm{B} T_\mathrm{g})$.

Table 3: Input parameters

Term	Symbol	Value	Unit
Temperature of background gas	T_g	10^3	K
Pressure of background gas	p	10^4	Pa
Distance between two electrodes	L	2×10^{-3}	m
Voltage applied on the cathode		-350	V
Voltage applied on the anode		0	V
secondary emission coefficient	γ_i	0.2	

4.2.2. Results of the plasma model

In this section the results of the plasma model and the comparison of the results from CFS and EDS will be presented.

First we present the solutions obtained from a very fine grid (the number of grid points is 2561) in figure 4(a) and 4(b) for the particles densities and potentials and electric fields, respectively. We can see that the results from the two schemes are very closed to each other. In addition, the grid is so fine that the results from a finer grid almost coincide with these, and as a result, we can regard the solutions as the exact solutions and later we use them as the references to compare the accuracy of CFS and EDS.

With the solutions shown in figure 4 we calculate the discretization errors of the solutions obtained on various girds. The grid size is halved each time. The maximum of the discretization errors for the two schemes is shown in table 4.

In order to observe the variation of the errors with the grid sizes the maximum of the discretization errors as a function of the grid sizes is plotted in a log-log graph in figure 5.

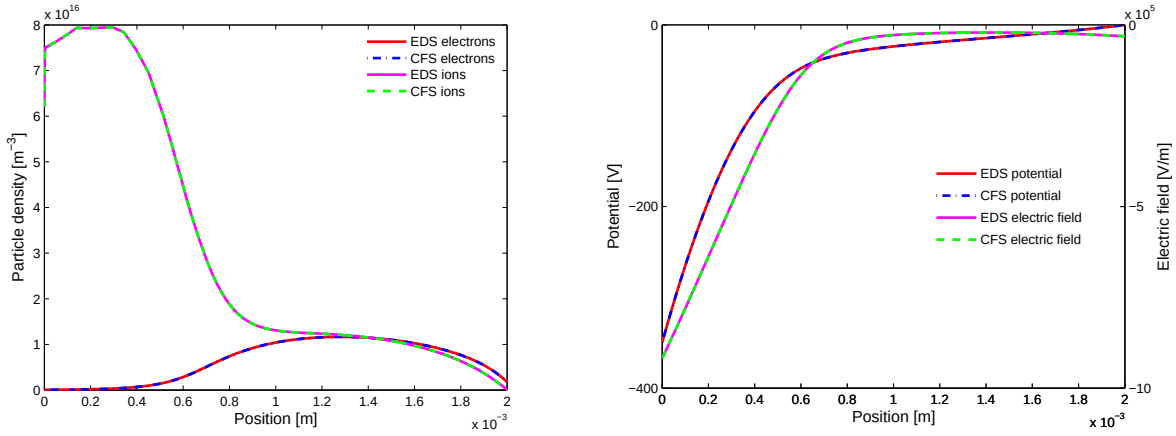

(a) particle densities (b) potential and electric field

Figure 4: Spatial variations of the particle densities (a) and the potential and electric field (b) obtained from CFS and EDS.

Table 4: The maximums of the discretization errors of the solutions from CFS and EDS. $N+1$ is the number of grid points.

	CFS		EDS	
$N+1$	ions density	electrons density	ions density	electrons density
21	4.5403e+15	1.2693e+15	4.2838e+15	4.4665e+14
41	1.1004e+15	3.0260e+14	1.9051e+15	2.8835e+14
81	2.9050e+14	7.5057e+13	9.9332e+14	1.4536e+14
161	7.2004e+13	1.8047e+13	4.7629e+14	6.4722e+13
321	1.8027e+13	4.0043e+12	1.9223e+14	2.4294e+13
641	4.2504e+12	8.6030e+11	6.1651e+13	7.4654e+12
1281	1.1993e+12	1.6773e+11	1.6923e+13	2.0249e+12

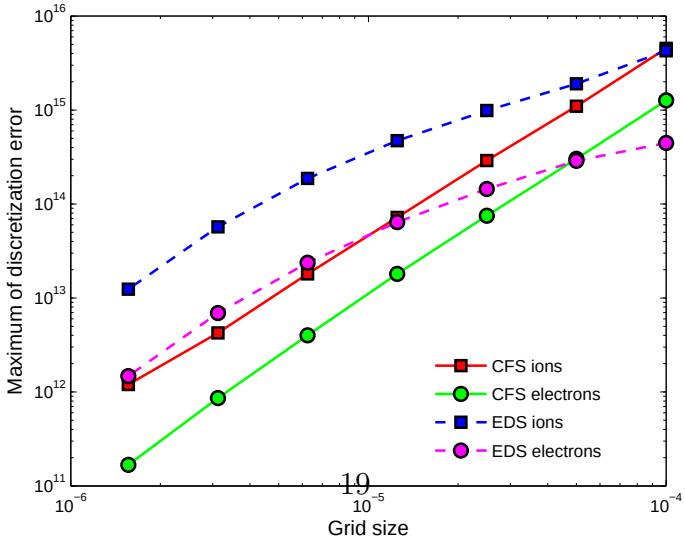

Figure 5: Log-log graph. The maximum of the discretization error as a function of the grid size h.

The slopes of the curves from CFS are approximately 2, while those of EDS change approximately from 1 to 2 as the grid size decreases. This demonstrates that the solutions from CFS are second order accurate and those from EDS are first-order accurate when the grid size is relatively large, and second order accurate when the grid size is small. Although the discretization error of the solution of electrons from CFS is larger when the grid is coarse, it reduces faster as the grid size decreases. After the number of grid points exceeds 161 the discretization errors of the solutions from CFS are much smaller than those of EDS.

After comparing the accuracy of the two schemes we compare the efficiency of them. The CPU times of the two schemes for different number of grid points for 5000 time steps are recorded in table 5. We can see that CFS doesn't cost much more extra CPU time, although its numerical flux has two additional terms related to the source term. The extra time is about 10% and it decreases as the number of grid points increases. If we compare the discretization errors in figure 5 we can see that CFS only needs half (or less) the number of grid points of EDS to get a same level of accuracy. To illustrate this point, we plot the CPU time as a function of the discretization error of ions in figure 6. It shows that for a given accuracy the CPU time of CFS is much smaller than that of EDS; only when the grid is very coarse, they are more or less the same.

Table 5: CPU times of the two schemes for 5000 steps for different number of grid points.

N	T_{CFS} (s)	T_{EDS} (s)	$\frac{T_{\mathrm{CFS}}-T_{\mathrm{EDS}}}{T_{\mathrm{EDS}}}(\%)$
21	16.222	13.087	24
41	17.968	15.734	14
81	25.619	22.806	12
161	39.636	35.838	11
321	65.885	59.853	10
641	120.34	110.09	9.3
1281	225.90	207.41	8.9

5. Conclusions

We have analyzed the truncation and discretization errors for CFS, and proved that CFS has second order convergence for all grid Péclet numbers. Two case studies verified these theoretical results. For a typical gas discharge model we have found that the continuity equation of electrons is a diffusion-dominated problem even when the grid is coarse. The continuity equation of ions, on the contrary, is a drift-dominated problem even when the grid size is relatively small. This means that EDS is second order accurate for the continuity equation of electrons and first-order accurate for that of ions when the grid size is not small enough. Since both continuity equations are coupled through the electric field, the over-all solutions from EDS are first-order accurate, unless the grid spacing is very small, whereas CFS is uniformly second order accurate. As a result, we found that for a fixed number of

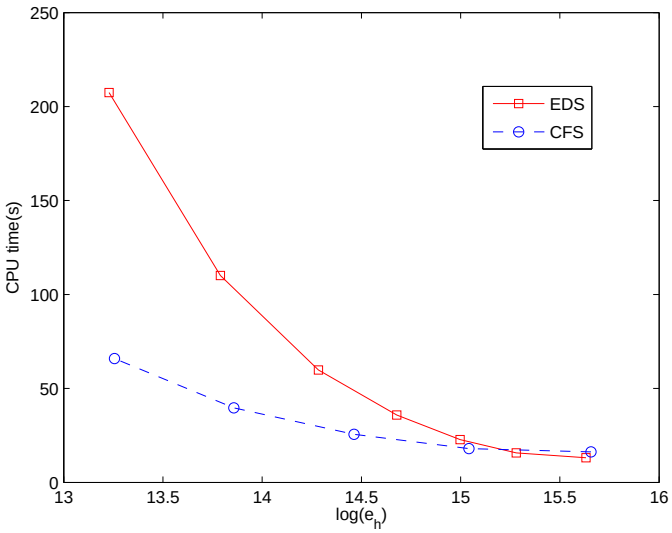

Figure 6: The CPU time as a function of the discretization error of ions.

grid points CFS yields a much higher accuracy, at the cost of only slightly more computer time.

Present and future work aims at the application of the scheme to higher-dimensional problems, for which the improved accuracy of CFS (or, stated differently, the need for fewer grid points) has an even greater impact.

The MATLAB/Octave code that has been used for the numerical experiments in this paper has been made available under the GNU General Public License (GPL) version 3. It can be found on the publisher's website.

6. Acknowledgements

The authors Lei Liu, Jan van Dijk and Diana Mihailova acknowledge the support by the Dutch Technology Foundation STW (project 10118). In addition, Jan van Dijk and Diana Mihailova also acknowledge the support by the CATRENE SEEL project (CA502).

References

[1] J. Singer, Combustion: Fossil Power Systems, 4th Edition, Combustion Engineering Power Systems Group, 1993.
[2] J. Bittencourt, Fundamentals of plasma physics, 3rd Edition, Springer, New York, 2010.
[3] F. Chen, Introduction to Plasma Physics and Controlled Fusion, 2nd Edition, Vol. 1, Springer, 1984.
[4] P. Yu, M. Cardona, Fundamentals of Semiconductors: Physics and Materials Properties, 4th Edition, Springer, 2010.
[5] D. Scharfetter, H. Gummel, Large-signal analysis of a silicon read diode oscillator, IEEE Trans. Electron Devices 16 (1969) 64–77.
[6] D. Spalding, A novel finite difference formulation for differential expressions involving both first and second derivatives, Plasma Sources Sci. Technol. 4 (1972) 551–559.

[7] J. ten Thije Boonkkamp, M. Anthonissen, The finite volume-complete flux scheme for advection-diffusion-reaction equations, J. Sci. Comput. 46 (1) (2011) 47–70. doi:10.1007/s10915-010-9388-8.
[8] T. El-Mistikawy, M. Werle, Numerical method for boundary layers with blowing-the exponential box scheme, AIAA J. 16 (1978) 749–751.
[9] M. Stynes, E. O'Riordan, A uniformly accurate finite element method for a singular perturbation problem in conservative form, SIAM J. Numer. Anal. 23 (2) (1986) 369–375.
[10] H.-G. Roos, M. Stynes, L. Tobiska, Robust numerical methods for singularly perturbed differential equations. Convection-diffusion-reaction and flow problems, 2nd Edition, Springer-Verlag Berlin Heidelberg, 2008.
[11] W. Hundsdorfer, J.G.Verwer, Numerical Solution of Time-Dependent Advection-Diffusion-Reaction Equations, Springer, 2003.
[12] J. ten Thije Boonkkamp, M. Anthonissen, The complete flux scheme for conservation laws in curvilinear coordinates, in: R. Petrova (ed) Finite Volume Method - Powerful Means of Engineering Design, InTech, Rijeka (2012) 83–100.
[13] P. Knabner, L. Angermann, Numerical Methods for Elliptic and Parabolic Partial Differential Equations, Springer, New York, 2003.
[14] R. Kellogg, A. Tsan, Analysis of some difference approximations for a singular perturbation problem without turning points, Math. Comp. (1978) 1025–1039.
[15] A. Berger, J. Solomon, S. L. M. Ciment, B. Weinberg, Generalized oci schemes for boundary layer problems, Math. Comp. 35 (1980) 695–731.
[16] A. Berger, J. Solomon, M. Ciment, An analysis of a uniformly accurate difference method for a singular perturbation problem, Math. Comp. 37 (1981) 79–94.
[17] D. Smith, The multivariable method in singular perturbation analysis, SIAM Rev. 17 (1975) 221–273.
[18] P. Wesseling, Principles of Computational Fluid Dynamics, Springer, Berlin, 2000.
[19] J.-P. Boeuf, A two-dimensional model of dc glow discharges, J. Appl. Phys. 63 (5) (1988) 1342–1349.
[20] G. Hagelaar, L. Pitchford, Solving the Boltzmann equation to obtain electron transport coefficients and rate coefficients for fluid models, Plasma Sources Sci. Technol. 14 (2005) 722–733.
[21] S. Conte, C. deBoor, Elementary Numerical Analysis, McGraw-Hill, New York, 1955.
[22] P. Ventzek, T. Sommerer, R. Hoekstra, M. Kushner, Two-dimensional hybrid model of inductively coupled plasma sources for etching, Appl. Phys. Lett. 63 (1993) 605–607.
[23] P. Ventzek, R. Hoekstra, M. Kushner, Two-dimensional modeling of high plasma density inductively coupled sources for materials processing, J. Vac. Sci. Technol. B 12 (1994) 461–477.
[24] G. Lapenta, F. Iinoya, J. Brackbill, Particle-in-cell simulation of glow discharges in complex geometries, IEEE Trans. Plasma Sci. 23 (4) (1995) 769–779.
[25] H. Gummel, A self-consistent iterative scheme for one-dimensional steady state transistor calculations, IEEE Trans. Electron Devices 11 (1964) 455–465.

PREVIOUS PUBLICATIONS IN THIS SERIES:

Number	Author(s)	Title	Month
12-23	L.M.J. Florack A. Fuster	Riemann-Finsler geometry for diffusion weighted magnetic resonance imaging	June '12
12-24	G.A. Bonaschi O. Filatova C. Mercuri A. Muntean M.A. Peletier V. Shchetnikava E. Siero I. Zisis	Identification of a response amplitude operator for ships	July '12
12-25	C.I. Gheorghiu M.E. Hochstenbach B. Plestenjak J. Rommes	Spectral collocation solutions to multiparameter Mathieu's system	July '12
12-26	P.A. Absil M.E. Hochstenbach	A differential-geometric look at the Jacobi-Davidson framework	July '12
12-27	L. Liu J. van Dijk J.H.M. ten Thije Boonkkamp D.B. Mihailova J.J.A.M. van der Mullen	The complete flux scheme – error analysis and application to plasma simulation	July '12

Ontwerp: de Tantes,
Tobias Baanders, CWI